PCCP

Accepted Manuscript

ROYAL SOCIETY OF CHEMISTRY

www.rsc.org/pccp

Cite this: DOI: 10.1039/c0xx00000x

www.rsc.org/xxxxxx

ARTICLE TYPE

Deactivation Mechanism of a Novel AIE-active Naphthalimide Derivative in More Polar Solutions

Yunqing Chen ‡ [a], Yi Wang ‡ [a], Yuan Yuan [b], Yan Jiao [a], Xuemei Pu [a,] * and Zhiyun Lu [a,] *

Received (in XXX, XXX) Xth XXXXXXXXX 20XX, Accepted Xth XXXXXXXXX 20XX

DOI: 10.1039/b000000x

Aggregation-induced emission (AIE) compounds with intramolecular charge transfer (ICT) character have attracted considerable interests from experimental and theoretical researchers due to their potential in optoelectronic and sensory applications. However, their deactivation mechanism in solutions has been disputed, limiting their further applications. Therefore, in this work, we combined experimental observations with density functional theory (DFT) and time-dependent DFT (TD-DFT) methods to unveil the deactivation mechanism of a new AIE-active naphthalimide derivative (FNIb) in the polar solution, which was synthesized by us lately. An in-depth investigation on the effects of the solvent polarity on its geometrical and electronic structures, absorption and emission spectra indicates that FNIb would prefer a conformational planarization mechanism to a popular twisted intramolecular charge transfer mechanism (TICT) in the deactivation process. Our findings would add more insights into previous studies to rationalize the controversy on the deactivation mechanism of the AIE ICT-featured compounds in solutions.

1. Introduction

Recently, a unique photoluminescence (PL) behaviour namely aggregation-induced emission (AIE) has attracted extensive attention and turned into a hot research issue.[1-5] Typical AIE-active fluorogens are non-emissive in dilute solutions but highly luminescent upon aggregation.[6] In addition, some donor-acceptor (D−A) systems exhibited AIE-active only in specific solvents like highly polar aqueous solutions and their solid-state efficiencies are still lower than those of molecularly dissolved species in nonpolar solvents.[7, 8] They are called as selective AIE fluorogens.[9] Either typical AIE-active fluorogens or selectively AIE-active ones have provided an effective solution to the thorniest aggregation-induced fluorescence quenching (AIQ)[10-12] problem of luminogens in solid state light-emitting applications.[13] Additionally, the characteristics of fluorescence ON/OFF switch of AIE luminogens[14] make them promising candidates in sensory systems.[15, 16] Most AIE compounds reported so far bear 1,1,2,2-tetraphenylethene (TPE) and multiphenylsilole fluorogens with propeller-shaped conformations,[17] so that they could undergo intense intramolecular rotations in solution, leading to drastically quenched PL emission, while their aggregates show strong fluorescence due to the restriction of their intramolecular rotations (RIR).[18-20]

Although the RIR mechanism currently dominates the AIE compounds, for AIE-active luminogens with donor-acceptor (D-A) structure, their efficient fluorescence quenching in polar solvents was generally ascribed to the twisted intramolecular charge transfer (TICT) mechanism. Nevertheless, with regard to the this mechanism, there has been a matter of dispute about how the twisting motion happens and what kind of conformation would the rotation result in, since the direct measurement of the configurations of the exited state of the luminogens is experimentally difficult. Consequently, considerable efforts from both experimental and computational aspects have been devoted to solve this problem. Nowadays, two different models have been proposed by different groups to explain the AIE mechanism for the ICT-featured AIE compounds i.e., TICT and conformational planarization. [21-28]

In the TICT model,[21-23] its characteristic feature lies in the rotation around the single bond connecting the D and A units after a completely intramolecular charge-transfer (ICT) procedure in the molecule, so that the D moiety is perpendicular to the A group, leading to radiative transition with forbidden nature. While for the conformational planarization mechanism,[24-28] the planarization of the whole molecule, especially the pyramidal diphenylamine group, is the most important feature, which would result in an increase on the efficiency of the internal conversion deactivation channel, thus blocking the radiative pathway. Although the AIE-active properties of most ICT-featured D-π-A compounds have been ascribed to the TICT model,[29] studies supporting a planar molecule skeleton have been continually proposed in recent years. The ambiguous mechanism of these ICT-AIE compounds significantly limits the rational design of high performance CT-featured AIE compounds.

Recently, we have developed a novel AIE active red D-π-A naphthalimide derivative FNIb for solid state lightening applications,[30] its molecular structure is shown in Fig. 1, where (fluoren-2-yl) diphenylamine acts as the D subunit, ethenylidene as the π-bridge, and 7*H*-benzimidazo[2,1-*a*]benzo[*de*] isoquinolin-7-one as the A subunit. Similar to most AIE D-π-A

fluorophores, the PL emission of FNIb was found to be drastically quenched in more polar aprotic solvent like dichloromethane (DCM), acetonitrile and DMSO, consequently, we tentatively attributed its AIE mechanism to the effective restriction of the TICT process in condensed state. However, as both TICT and conformational planarization may account for the AIE phenomenon of FNIb, to clarify its AIE mechanism, herein, we studied the effect of the solvent polarity on the geometric and electronic structures, absorption and fluorescence properties, and the potential energy surface for the ground and excited states of FNIb through both experimental observations and theoretical methods, while cyclohexane (CHX) and dichloromethane (DCM) were selected as representatives of aprotic non-polar and polar media.

We hope that the observations from the work could reveal the microscopic origin of the novel luminescent behaviors of FNIb in solutions so that the useful information can be obtained for the application environment of fluorenonearylamine derivatives like FNIb and rationalizing the controversy on the deactivation mechanism of the AIE compounds.

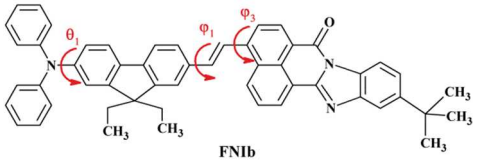

Fig. 1 The molecular structure of FNIb

2. Methods

2.1 Experimental details

FNIb studied in the work was prepared according to our previously published procedures.[30] The UV-vis absorption and emission spectra were obtained in cyclohexane (CHX), and dichloromethane (DCM). Absorption spectra were measured on a Perkin-Elmer Lambda 950 scanning spectrophotometer in dilute solutions and the PL emission spectra of both solution and thin-film samples were recorded on a Perkin-Elmer LS55 fluorescence spectrophotometer at room temperature.

2. 2 Computational details

We have followed a well-established four-step approach: (i) to optimize the ground and excited state geometries in the gas-phase and the two selected solvents; (ii) vibrational frequency calculations confirm that the optimized structure is a true minimum on the potential energy surface; (iii) from the optimized ground and excited state geometries to obtain the absorption and emission spectra in two kinds of solvents using time dependent DFT (TD-DFT) approach;[31] (iv) the exploration of excited states' potential energy surface (PES) in dichloromethane (DCM).

In order to select reasonable computation levels for the structure optimization on the ground and excited states, five wildly used hybrid density functional theory (DFT) functionals (viz., PBE0, B3LYP, CAM-B3LYP, wB97XD and BP86)[32-36] with 6-31G(d,p) basis set were considered. Due to unavailable X-ray structure of FNIb, we selected the most appropriate computation level from the five DFT functionals above to optimize FNIb molecule in terms of the correlation between the experimental spectrum data with the calculated ones derived from the optimized structure (see Table 1). The results showed that the best agreements between the experimental spectrum data and the calculated ones were obtained at the level of BP86/6-31G (d,p) for the ground-state optimization and B3LYP/6-31G(d,p) for the lowest singlet excited-state optimization. The frequency and frontier orbital calculations were performed at the same level as the corresponding optimizations. Based on optimized geometries, TD-DFT calculations were carried out at the level of M06-2X/6-31G(d,p) to obtain the absorption and emission spectra, since the M06-2X method[5] has been demonstrated to give a good agreement with experimental spectra in this kind of aniline derivatives. The relaxed PES scans of FNIb in DCM were carried out with four DFT functionals (viz., PBE0, B3LYP, CAM-B3LYP and BP86) at the level of 6-31G(d) to ensure the reliability of the results.

All calculations above but gas-phase included the corresponding solvent environment using the polarizable continuum model (PCM).[37, 38] All calculations have been performed with the Gaussian09 package of programs.[39]

Table 1: Computed absorption and emission maxima (nm) of FNIb in DCM [a]

Methods[b]	λ_{abs}/nm	λ_{em}/nm
EXP [c]	468	664
BP86	459	890
B3LYP	433	676
CAM-B3LYP	403	607
PBE0	554	677
WB97XD	338	608

[a] The absorption and emission maxima of FNIb in DCM were calculated using TDDFT method at the level of M06-2X/6-311G (d,p), based on the optimized S_0 and S_1 structures, respectively; [b] Optimization functionals; [c] Experimental values in DCM.

3. Results and Discussion

3.1 Spectral data of Experiments

Table 2 and Fig. 2 show the spectral data measured. As can be seen, FNIb exhibits a maximum absorption at 457 nm in CHX and is slightly red-shifted to 468 nm in DCM, suggesting that the solvent polarity plays a minor role in the variation of the absorption spectra of FNIb. In contrast, the luminescence behavior of FNIb displays a significant difference due to the change of the solvent polarity. The colors of the fluorescence change from light green in CHX to deep red in DCM. FNIb emits at 530 nm with a fluorescence quantum yield (Φ_F) of 75% in CHX, while a main emission band peaked at 655 nm is observed in DCM with only 0.5% of the Φ_F value. In other words, the emission becomes nearly invisible in the polar DCM media. Evidently, the emission of FNIb presents a bathochromical-shifted behavior and a remarkable drop in intensity with increasing the solvent polarity. The observation clearly indicates that FNIb possesses selectively AIE-active characteristic only in the polar media. Thus, it should be ascribed to the selective AIE fluorogens.

3.2 Computational Analysis

3.2.1 Geometrical Structures

As known, spectral behaviors are closely associated with the

Table 2: Summary of the experimental and theoretical spectral values, the absorption and emission maxima (λ), oscillator strength (*f*), main configurations of the transition and transition energies (TE/eV) in gas-phase and two different solvents, calculated at the level of M06-2X/6-311G (d,p) using TDDFT method.

system	S_0-abs [a]			S_1-flu [b]		
media	GAS	CHX	DCM	GAS	CHX	DCM
λ_{exp}/nm		457	468		539	664
λ_{cal}/nm	435	451	458	497	521	678
Main configurations	H->L (61%) H-1->L (27%)	H->L (61%) H-1->L (28%)	H->L (62%) H-1->L (28%)	H->L (53%) H-1->L (39%)	H->L (79%) H-1-> (16%)	H->L (91%)
f	1.85	1.97	1.93	1.10	1.43	1.17
TE/eV	2.85	2.74	2.70	2.51	2.38	1.83
Φ_{PL} [c]					0.75	0.005

[a] The BP86/6-31G (d,p) S_0 structure was used; [b] The B3LYP/6-31G (d,p) S_1 structure was used. [c] The fluorescence quantum yields derived from the experimental determination. (Assignment: H=HOMO, L=LUMO, H-1=HOMO-1)

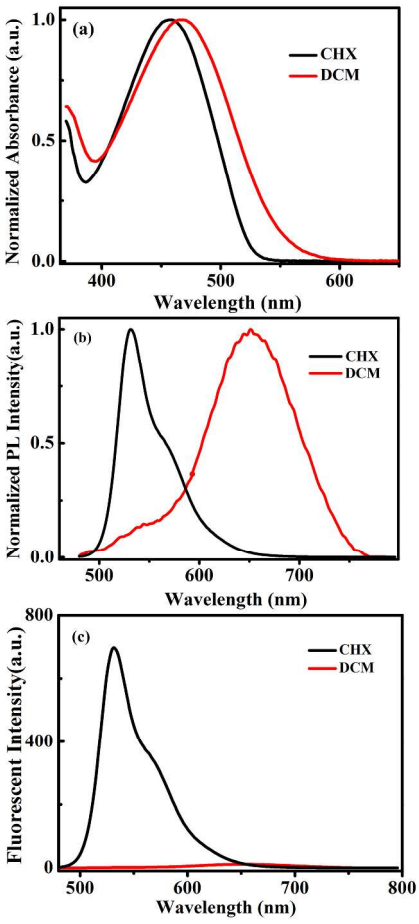

Fig. 2 (a) Normalized absorption and (b) fluorescence spectra of FNIb in CHX and DCM at 298 K. (c) Fluorescence spectra of FNIb in CHX and DCM at 298 K. Excitation wavelength is 460 nm.

molecular structures.[40] Thus, we optimized FNIb structures in the ground state and the excited one for vacuo and the two different solvent environments at the level of BP86/6-31G(d,p) and B3LYP/6-31G(d,p), respectively (see the part of computational method for the selection of the computational level). Some important geometrical parameters calculated are summarized in Table 3, in which atoms are labelled according to Fig. 3.

Since slightly pyramidal amino nitrogen is an important feature of the aniline derivatives, we concerned three dihedral angles associated with the amino nitrogen, namely, θ_1, θ_2 and θ_3. Besides, the dihedral angles φ_1, φ_2 and φ_3 involved in the π bridge were also taken into accounts, which play a major role in influencing the conformation of donor and accepter subunits. For the ground state geometry, the six dihedral angles nearly have no changes with the increase of the solvent polarity. Similarly, the solvent polarity hardly affects the important bond lengths in the ground structure. In a whole, the solvent effect contributes little to the structural changes of the ground state.

Compared to the ground states, the geometrical structures of the first excited states are significantly affected by the polarity of solvents, in particular for θ_1, θ_2 and φ_1. The dihedral angle θ_1 ranges from 44.2° in gas-phase to 37.0° in CHX, and to 31.8° in DCM, displaying a trend of planarization of the donor part. Similar change is observed for θ_2. In contrast, φ_1 presents a slight rise with increasing the solvent polarity from 162.7° in gas-phase to 165.2° in CHX, and to 168.2° in DCM. For the other dihedral angles, no significant changes are observed. In addition, the bond length of N_1-C_{11} (R_1) involved in the amino nitrogen is shortened significantly upon the increase in the solvent polarity. In DCM media, the bond length of R_1 is calculated to be 1.396 Å, close to the bond length of C=N double bond.[41] The similar variation trends are also observed for the bond lengths of C_4-C_{14} (R_5) and C_{15}-C_{37} (R_7) involved in the π bridge. The shortened bond length implies that the conjugated system of the molecule would be enhanced with increasing the solvent polarity. The structural observations above clearly show that the geometries of the excited state tend to be coplanar with the rise of the solvent polarity, rather than approach a perpendicular structure observed in many other D-π-A emitters.

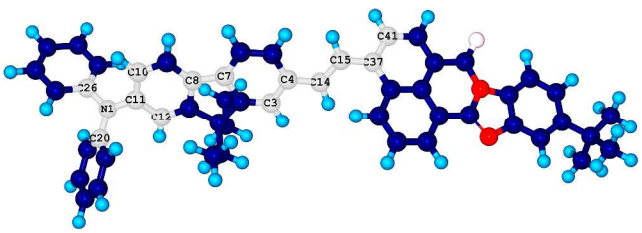

Fig. 3 The atomic labels of FNIb

Table 3: Selected geometrical parameters (bond length in Å, angle and dihedral angle in degrees) and some frontier orbital energies (eV) of the ground and the first excited states of FNIb in two different solvents and vacuo

system	S_0 [a]			S_1 [b]		
Geometrical Parameters	GAS	CHX	DCM	GAS	CHX	DCM
θ_1 (C_{26}-N_1-C_{11}-C_{10})	36.78	36.65	36.43	44.20	37.01	31.81
θ_2 (C_{20}-N_1-C_{11}-C_{12})	36.15	35.96	35.74	43.95	36.54	31.24
θ_3 (C_{26}-C_{20}-C_{11}-N_1)	0.32	0.34	0.33	0.12	0.25	0.19
R_1 (N_1-C_{11})	1.420	1.419	1.419	1.423	1.407	1.397
R_2 (N_1-C_{26})	1.427	1.427	1.427	1.411	1.419	1.425
R_3 (N_1-C_{20})	1.427	1.428	1.428	1.413	1.420	1.426
R_4 (C_7-C_8)	1.462	1.462	1.461	1.457	1.451	1.444
φ_1 (C_3-C_4-C_{14}-C_{15})	167.91	168.42	169.61	162.72	165.19	168.20
φ_2 (C_4-C_{14}-C_{15}-C_{37})	177.14	177.25	177.39	177.37	178.11	178.37
φ_3(C_{14}-C_{15}-C_{37}-C_{41})	145.48	145.68	146.22	156.01	155.93	156.63
R_5 (C_4-C_{14})	1.460	1.459	1.459	1.461	1.457	1.450
R_6 (C_{14}-C_{15})	1.366	1.367	1.368	1.363	1.366	1.370
R_7 (C_{15}-C_{37})	1.461	1.461	1.460	1.449	1.448	1.443
			Energies of the frontier orbitals (eV) [c]			
HOMO-1	-6.96	-7.01	-7.09	-6.91	-6.96	-7.03
HOMO	-6.32	-6.30	-6.33	-6.29	-6.24	-6.22
LUMO	-2.19	-2.25	-2.34	-2.37	-2.40	-2.49
$\Delta E_{(HOMO-1-LUMO)}$	4.77	4.76	4.75	4.54	4.56	4.54
$\Delta E_{(HOMO-LUMO)}$	4.12	4.05	3.99	3.92	3.83	3.72

[a] Optimized at the level of bp86/6-31G (d,p); [b] Optimized at the level of b3lyp/6-31G (d,p); [c] calculated at the level of M06-2X/6-311G (d,p).

3.2.2 Calculated Spectrum and Frontier Orbital Analysis

Based on the S_0 and S_1 geometries optimized, TD-DFT method was used to calculate the spectral properties of FNIb in gas phase and the two solvents at the level of M06-2X/6-311G(d,p) within the framework of PCM. The calculated results are summarized in Table 2, along with the selected experimental data. In addition, the frontier molecular orbitals of S_0 and S_1 were further calculated at the level of M06-2X/6-311G(d,p). Fig. 4 displays the electronic densities of main frontier molecular orbitals.

3.2.2.1 Absorption spectra

As shown in Table 2, the strongest absorption band obtained in experiment is located at 468 nm in DCM, which well matches the calculated value of 458 nm. And the computed absorption band at 451 nm in CHX also well reproduces the experimental data of 457 nm. The good consistency between the calculated data and the experimental ones confirms that the computation level adopted in the work is reliable.

The data in Table 2 indicate that the strong adsorption bands are mainly dominated by the highest occupied molecular orbital (HOMO), HOMO-1, the lowest unoccupied molecular orbital (LUMO) and are mainly of a HOMO->LUMO character with a relatively weak contribution from HOMO-1->LUMO transition. As shown in Fig. 4, the differences in the electron densities of these frontier orbitals between the different solvents are very slight for the ground (S_0) structures. HOMO orbitals were primarily localized over the donor (D) and π-Bridge (π) moieties while the electronic densities of HOMO-1 orbitals were almost distributed all over the whole molecules. The LUMO orbitals are mainly centered on the π-bridge (π) and acceptor (A) moieties. These observations confirm that FNIb has a character of intramolecular charge transfer (ICT) like most of D-A/D-π-A compounds.[42-44] In addition, the HOMO and LUMO orbitals exhibit π and π* characters, respectively, as reflected by Fig. 4. Thus, the HOMO–LUMO transition can be attributed to π-π* intramolecular charge transfer.

As can be seen from Table 3, the solvents play a negligible role in influencing the energy of the HOMO orbital in the S_0 state. However, the solvent polarity lowers the energies of LUMO and HOMO-1. As result, the energy gaps of HOMO–LUMO are decreased when going from vacuo (4.12 eV) to CHX (4.05 eV) to DCM (3.99 eV). While $\Delta E_{(HOMO-1–LUMO)}$ is nearly unchanged. As a result, the intensive absorption peaks contributed from the HOMO-LUMO and HOMO-1-LUMO transitions only exhibit slight red-shift with increasing solvent polarity, as observed in Figs. 2a-2b.

3.2.2.2 Emission spectra

The data in Table 2 show that the strong emission bands calculated also reproduce the experimental values. For example, the emission spectrum of FNIb in CHX is dominated by a band at 539 nm, which is corresponded to a computed maximum band of 521 nm. The emission peak in the CHX solvent includes 79 % contribution from HOMO–LUMO transition and 16% contribution from HOMO-1->LUMO. In DCM, the experimental

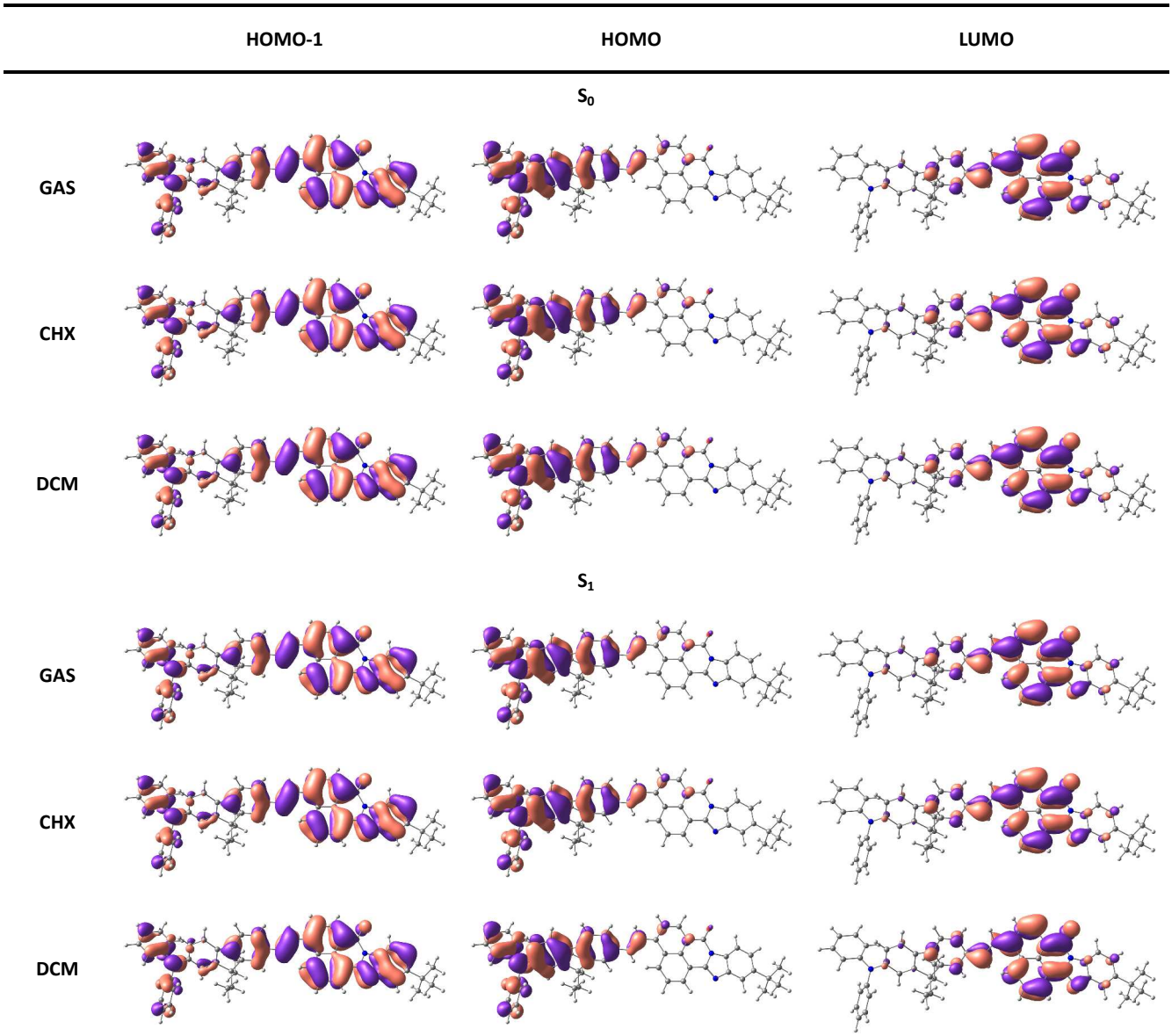

Fig. 4: Representation of the molecular orbitals involved in the electronic transitions both in adsorption and emission spectra.

emission peak at 664 nm is calculated to be 678 nm and is almost contributed from HOMO–LUMO transition (90%). The electronic density distributions over HOMO, HOMO-1 and LUMO in the S_1 states are similar to those in the S_0 ones, which also display a pronounced ICT and π->π* transition characters. Similarly, the solvent polarity also lowers the energies of HOMO-1 and LUMO in the excited states. However, different from the ground-state, an observable rise upon increase of the solvent polarity is presented for the energies of HOMOs in the S_1 states. As a result, the HOMO–LUMO energy gaps of the S_1 state decreased from 3.92 eV in gaseous phase to 3.83 eV in CHX and 3.72 eV in DCM (see Table 3). While the solvent polarity hardly affects the energy gaps of HOMO-1-LUMO transitions in the S_1 state, similar to the S_0 state. Compared with the S_0 state, the main emission bands of the S_1 state have more contributions from HOMO-LUMO transitions in the solvent environment and the contributions are enhanced by the solvent polarity. In the DCM media, the contribution from HOMO-LUMO transition is high up to be 90%. Thus, the strong solvatochromic behavior is observed in the fluorescence spectra due to the lowered energy gaps of HOMO-LUMO upon the increase of the solvent polarity. As observed above, the adsorption spectra only exhibits a slight red shift with increasing solvent polarity since it has more contributions from HOMO-1-LUMO while the energy gaps of HOMO-1-LUMO transitions in the ground state almost remain unchangeable despite of the change in solvent polarity. The observation further indicates that the solvent effect on the S_1 state is stronger than S_0.

3.2.3 Mechanism of Radiationless Decay

As mentioned above, the intramolecular rotation is active in the solutions, which would serve as a relaxation channel for the excited state to decay. However, there has been a continuing

controversy regarding the deactivation mechanism of AIE compounds in solutions. Which model should the decay mechanism of FNIb be described to in the polar DCM solvent: TICT or Planarization.

As revealed for the naphthalimide derivatives possessing D-π-A structure,[45] the most remarkable feature of TICT model is a significant twist of the donor-acceptor single bond and a large rotation between the benzene carbon and amino nitrogen atoms on the structures of first excited state. Thus, to explore the TICT hypothesis for FNIb in the polar solvent DCM, the scan of the relaxed potential energy surfaces (PES) were carried out for the three torsion angles involved the two regions (viz., θ_1, φ_1 and φ_3) of the first excited state in DCM, calculated at the level of B3LYP/6-31G (d) (see Fig.5). Additionally, the other four functionals (BVP86, CAM-B3LYP, wb97xd and PBE0) were also tested (Fig. 6) in the PES scans in order to ensure the reliability of the results calculated since some investigations pointed out that different functionals would lead to different potential energy surfaces.[7, 22, 25, 46]

As reflected by Fig.6, the four different functionals give qualitatively consistent results that almost all perpendicular conformations of S_1 at 90° appear to be the maximum on the PES curves, rather than the minimum. The PES curve of the twisted θ_1 indicates that the most stable dihedral angle appears at about 40°. The twisting dihedral angles φ_1 and φ_3 on the π-bridge exhibit the minimums at about 160°. As shown in Table 3, the structure of S_1 fully optimized at the level of B3LYP/6-31G(d,p) in DCM shows that the dihedral angles of θ_1, φ_1 and φ_3 are 31.2°, 168.2° and 156.6°, respectively, consistent with the observations from the PES curves above. Thus, the large torsion on the structures is not required to stabilize the ICT state of FNIb in DCM. Instead of adopting a twisted conformation, a relatively planar conformation seems more preferable.

In addition, some studies on the TICT model also proposed that the torsion of the molecular would lead to a stabilization of S_2 state and a destabilization of S_1 and S_0 states at 90°, exhibiting a canonical crossing of S_2 and S_1 states in the PES curves.[47, 48] Thus, to check the assumption, the relaxed PES scans were performed for the three dihedral angles of θ_1, φ_1 and φ_3 in the S_0 and S_2 states at the level of B3LYP/6-31G(d) in DCM, based on their corresponding optimized structures (see Fig.6). Similarly, the S_0 and S_2 states also exhibit the highest energy rather than the lowest energy at 90°, which does not follow the torsion way of TICT.

To gain more insight into the decay mechanism of FNIb in DCM solvent, we further analyze the electronic transition from the S_1 state to the S_0 one. In terms of the Franck-Condon principle, the fluorescence quantum yields (Φ_F) can be expressed as $\Phi_F=\kappa_r/(\kappa_r+\kappa_{nr})$,[49-51] in which κ_r and κ_{nr} are the radiative and nonradiative decay rates, respectively. The κ_r can be evaluated in terms of a simple formula $\kappa_r=fE^2/1.499$ derived from the Einstein spontaneous emission relationship. Herein, f denotes the oscillator strength of emission and E denotes the transition energy of the emission in cm^{-1}. According to the Franck-condon principle,[52-55] the nonradiative decay is dependent on the energy gap between the S_0 and S_1 states, which is closely associated with the relaxation from higher vibrational states to the lowest vibrational state. Such relaxation would cause a rearrangement of the molecular structure while the reorganization energy can be served as one indicator to characterize the value of κ_{nr}.[56-59] The larger the reorganization energy, the easier the nonradiactive transition between S_1 and S_0 would occur. Thus, we calculated the reorganization energy (E_R) in order to qualitatively estimate κ_{nr}.

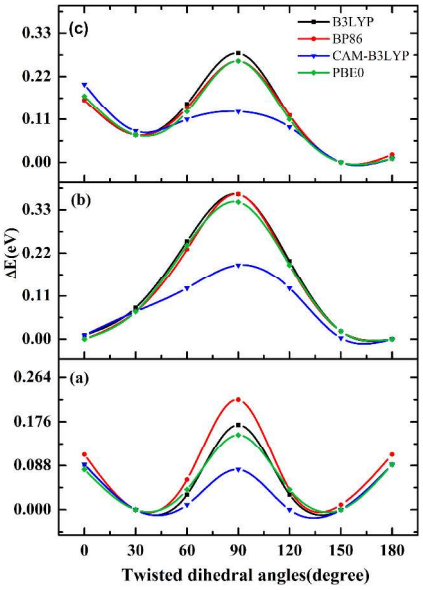

Fig. 5: Calculated potential-energy curves of the first excited state in DCM, potted as a function of the twisting dihedral angles θ_1 (a), φ_1 (b), φ_3 (c) for different functionals.

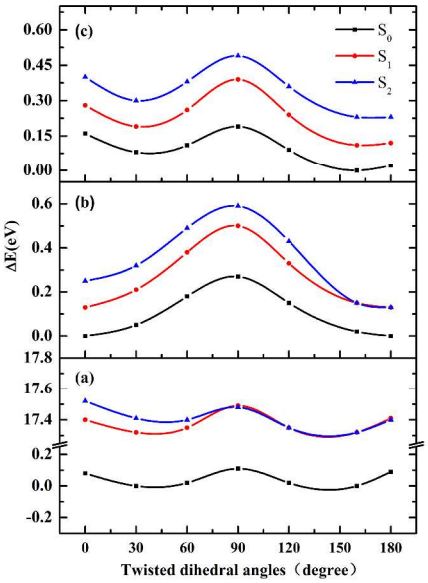

Fig. 6: Calculated potential-energy curves of S_0, S_1 and S_2 in DCM, potted as a function of the twisting dihedral angles θ_1 (a), φ_1 (b), φ_3 (c) at the level of B3LYP/6-31G (d).

Table 4: Emission data for FNIb in CHX and DCM, calculated at the level of M06-2X/6-311G (d,p)

	f^a	E^b/cm^{-1}	$\lambda_{em}{}^c$/nm	$\kappa_r{}^d$	$E_R{}^e$/eV
CHX	1.43	19157	522	3.50×10^8	0.502
DCM	1.17	14771	677	1.70×10^8	1.002

[a] oscillator strengths of emission; [b] transition energy; [c] maxima of the emission spectrum; [d] radiative rates; [e] reorganization energies.

Table 4 lists the calculated f, E, E_R and κ_r values. Due to smaller transition energy (E) in the polar DCM solvent, the κ_r in DCM is calculated to be 1.70×10^8 s^{-1}, much lower than 3.50×10^8 s^{-1} in CHX, which should contribute to lower Φ_F in DCM. The reorganization energy E_R in DCM solvent is calculated to be 1.002 eV, significantly larger than 0.502 eV in CHX media. The observation is consistent with previous findings that the increase in the solvent polarity would stabilize the ICT state and lowers the energy barrier of the reorganization.[60-62] Indeed, the six dihedral angles in the S1 state exhibit a trend to approach the planarization from gas phase to the nonpolar CHX to polar DCM, as shown in Table 3, which provides a structural support for the larger change in the ICT state induced by the polar DCM than the nonpolar CHX. Thus, larger E_R is observed in DCM solvent, implying more nonradiative energy loss by the structural relaxation, which leads to a larger κ_{nr} compared to non-polar CHX. Derived from smaller κ_r and larger κ_{nr} in DCM observed above, it can be predicted that the Φ_F of FNIb in DCM should be much lower than that in CHX, consistent with the experimental finding that the Φ_F of FNIb is sharply decreased from 0.75 in CHX to 0.005 in DCM.

In a whole, the observations above do not support the TICT decay mechanism in the polar DCM. Instead, the planarization model is more preferable.

Conclusions

Combining the experimental determinations with the computational analyses, we selected the two solvents (viz., cyclohexane (CHX) and dichloromethane (DCM)) to investigate the effect of the solvent polarity on the new kind of D–π-A fluorenonearylamine derivative (FNIb) possessing the selectively AIE-active characteristic in the polar media, which was lately synthesized by us. Our main objective is to clarify its deactivation mechanism in the polar solution, which has been a controversial issue on the AIE systems. The geometric structure and the potential energy surface curves do not support the popular TICT mechanism proposed for many traditional D–π-A structures. Instead, the deactivation mechanism would prefer to the conformational planarization for FNIb. Our results show that the increase in solvent polarity would facilitate the compound to approach planarization, leading to a narrower energy gap between HOMO and LUMO orbitals and larger reorganization energy in the S1 state. As a result, the significant red-shift emission, the decrease in the radiative decay rate and the increase in the non-radiative decay rate are observed with increasing the solvent polarity, which would lead to the occurrence of deactivation of FNIb in the polar DCM solvent.

The present results suggest that the conformational planarization model could be adopted to rationalize the deactivation of the novel AIE-active fluorenonearylamine derivatives in solution and the TICT model could not characterize the whole D–π-A AIE systems. We hope that the observations from this work can be helpful for the applications of this kind of materials and inspire further investigations on the decay mechanism of the other AIE systems.

Acknowledgment

This project is supported by the National Science Foundation of China (Grant No. 21273154, U1230121, 21372168).

Notes

[a] *Faculty of Chemistry, Sichuan University, Chengdu, Sichuan 610064, People's Republic of China. Fax: 86 028 8541 2290; Tel: 86 28 8541 2290; E–mail: xmpuscu@scu.edu.cn; zhiyunlu@scu.edu.cn.*

[b] *College of Management, Southwest University for Nationalities, Chengdu, Sichuan 610041, People's Republic of China. E–mail: 9520831@qq.com.*

‡ These authors contributed equally to this work.

References

1. Y. Hong, J. W. Lam and B. Z. Tang, *Chem. Commun.*, 2009, 4332-4353.
2. Y. Hong, J. W. Lam and B. Z. Tang, *Chem. Soc. Rev.*, 2011, **40**, 5361-5388.
3. S. Chen, Y. Hong, Y. Liu, J. Liu, C. W. Leung, M. Li, R. T. Kwok, E. Zhao, J. W. Lam and Y. Yu, *J. Am. Chem. Soc.*, 2013, **135**, 4926-4929.
4. Z. Song, Y. Hong, R. T. Kwok, J. W. Lam, B. Liu and B. Z. Tang, *J. Mater. Chem. B*, 2014, **2**, 1717-1723.
5. Y. Zhao and D. G. Truhlar, *Theor. Chem. Acc.*, 2008, **120**, 215-241.
6. J. Luo, Z. Xie, J. W. Y. Lam, L. Cheng, B. Z. Tang, H. Chen, C. Qiu, H. S. Kwok, X. Zhan, Y. Liu and D. Zhu, *Chem. Commun.*, 2001, 1740-1741.
7. B. R. Gao, H. Y. Wang, Z. Y. Yang, H. Wang, L. Wang, Y. Jiang, Y. W. Hao, Q. D. Chen, Y. P. Li, Y. G. Ma and H. B. Sun, *J. Phys. Chem. C*, 2011, **115**, 16150-16154.
8. B. R. Gao, H. Y. Wang, Y. W. Hao, L. M. Fu, H. H. Fang, Y. Jiang, L. Wang, Q. D. Chen, H. Xia, L. Y. Pan, Y. G. Ma and H. B. Sun, *J. Phys. Chem. B*, 2010, **114**, 128-134.
9. W. Z. Yuan, Y. Gong, S. Chen, X. Y. Shen, J. W. Lam, P. Lu, Y. Lu, Z. Wang, R. Hu and N. Xie, *Chem. Mater.*, 2012, **24**, 1518-1528.
10. Z. Y. Wang, Y. Q. Tan, Y. Y. Gong, P. Lu, J. W. Lam, X. Y. Shen, C. Feng, H. Y. Sung, Y. Lu, Y. Zhang and B. Z. Tamg, *Adv. Mater.*, 2013, **25**, 2837-2843.
11. R. M. Duke, E. B. Veale, F. M. Pfeffer, P. E. Kruger and T. Gunnlaugsson, *Chem. Soc. Rev.*, 2010, **39**, 3936-3953.
12. X. Gu, G. Zhang and D. Zhang, *Analyst*, 2012, **137**, 365-369.
13. S. L. Lin, L. H. Chan, R. H. Lee, M. Y. Yen, W. J. Kuo, C. T. Chen and R. J. Jeng, *Adv. Mater.*, 2008, **20**, 3947-3952.
14. N. B. Shustova, B. D. McCarthy and M. Dinca, *J. Am. Chem. Soc.*, 2011, **133**, 20126-20129.
15. M. Wang, G. Zhang, D. Zhang, D. Zhu and B. Z. Tang, *J. Mater. Chem.*, 2010, **20**, 1858-1867.
16. S. W. Thomas, G. D. Joly and T. M. Swager, *Chem. Rev.*, 2007, **107**, 1339-1386.
17. Z. F. An, C. Zheng, R. F. Chen, J. Yin, J. J. Xiao, H. F. Shi, Y. Tao, Y. Qian and W. Huang, *Chem. -Eur. J.*, 2012, **18**, 15655-15661.
18. R. Hu, N. L. Leung and B. Z. Tang, *Chem. Soc. Rev.*, 2014, **43**, 4494-4562.
19. B. R. Gao, H. Y. Wang, Y. W. Hao, L. M. Fu, H. H. Fang, Y. Jiang, L. Wang, Q. D. Chen, H. Xia and L. Y. Pan, *J. Phys. Chem. B*, 2009, **114**, 128-134.

20. J. Chen and B. Z. Tang, in *Aggregation-Induced Emission: Fundamentals and Applications*, *Volumes 1 and 2*, John Wiley and Sons Ltd, 2013, 307-322.
21. R. Hu, E. Lager, A. Aguilar-Aguilar, J. Liu, J. W. Lam, H. H. Sung, I. D. Williams, Y. Zhong, K. S. Wong and E. Pena-Cabrera, *J. Phys. Chem. C.*, 2009, **113**, 15845-15853.
22. X. Y. Shen, W. Z. Yuan, Y. Liu, Q. Zhao, P. Lu, Y. Ma, I. D. Williams, A. Qin, J. Z. Sun and B. Z. Tang, *J. Phys. Chem. C*, 2012, **116**, 10541-10547.
23. Y. Qian, M. Cai, X. Zhou, Z. Gao, X. Wang, Y. Zhao, X. Yan, W. Wei, L. Xie and W. Huang, *J. Phys. Chem. C*, 2012, **116**, 12187-12195.
24. K. A. Zachariasse, S. I. Druzhinin, W. Bosch and R. Machinek, *J. Am. Chem. Soc.*, 2004, **126**, 1705-1715.
25. C. A. Guido, B. Mennucci, D. Jacquemin and C. Adamo, *Phys. Chem. Chem. Phys.*, 2010, **12**, 8016-8023.
26. S. I. Druzhinin, A. Demeter and K. A. Zachariasse, *Chem. Phys. Lett.*, 2001, **347**, 421-428.
27. X. H. Duan, X. Y. Li, R. X. He and X. M. Cheng, *J. Chem. Phys.*, 2005, **122**, 084314.
28. R. X. He and X. Y. Li, *Chem. Phys.*, 2007, **332**, 325-335.
29. A. Mishra, S. Sahu, N. Dash, S. K. Behera and G. Krishnamoorthy, *J. Phys. Chem. B*, 2013, **117**, 9469-9477.
30. Y. Wang, J. Zhou, X. Wang, X. Zheng, Z. Lu, W. Zhang, Y. Chen, Y. Huang, X. Pu and J. Yu, *Dyes Pigments*, 2014, **100**, 87-96.
31. R. E. Stratmann, G. E. Scuseria and M. J. Frisch, *J. Chem. Phys.*, 1998, **109**, 8218.
32. A. D. Becke, *J. Chem. Phys.*, 1993, **98**, 5648.
33. C. Adamo and V. Barone, *J. Chem. Phys.*, 1999, **110**, 6158.
34. T. Yanai, D. P. Tew and N. C. Handy, *Chem. Phys. Lett.*, 2004, **393**, 51-57.
35. J. D. Chai and M. H. Gordon, *Phys. Chem. Chem. Phys.*, 2008, **10**, 6615-6620.
36. J. T. Rives and W. L. Jorgensen, *J. Chem. Theory Comput.*, 2008, **4**, 297-306.
37. E. Cancès, B. Mennucci and J. Tomasi, *J. Chem. Phys.*, 1997, **107**, 3032.
38. B. Mennucci, E. Cances and J. Tomasi, *J. Phys. Chem. B*, 1997, **101**, 10506-10517.
39. M. J. Frisch, G. W. Trucks, H. B. Schlegel, G. E. Scuseria, M. A. Robb, J. R. Cheeseman, G. Scalmani, V. Barone, B. Mennucci, G. A. Petersson, H. Nakatsuji, M. Caricato, X. Li, H. P. Hratchian, A. F. Izmaylov, J. Bloino, G. Zheng, J. L. Sonnenberg, M. Hada, M. Ehara, K. Toyota, R. Fukuda, J. Hasegawa, M. Ishida, T. Nakajima, Y. Honda, O. Kitao, H. Nakai, T. Vreven, J. A. Montgomery Jr., J. E. Peralta, F. Ogliaro, M. J. Bearpark, J. Heyd, E. N. Brothers, K. N. Kudin, V. N. Staroverov, R. Kobayashi, J. Normand, K. Raghavachari, A. P. Rendell, J. C. Burant, S. S. Iyengar, J. Tomasi, M. Cossi, N. Rega, N. J. Millam, M. Klene, J. E. Knox, J. B. Cross, V. Bakken, C. Adamo, J. Jaramillo, R. Gomperts, R. E. Stratmann, O. Yazyev, A. J. Austin, R. Cammi, C. Pomelli, J. W. Ochterski, R. L. Martin, K. Morokuma, V. G. Zakrzewski, G. A. Voth, P. Salvador, J. J. Dannenberg, S. Dapprich, A. D. Daniels, Ö. Farkas, J. B. Foresman, J. V. Ortiz, J. Cioslowski and D. J. Fox, Gaussian, Inc., Wallingford, CT, USA2009.
40. G. Yu, S. Yin, Y. Liu, J. Chen, X. Xu, X. Sun, D. Ma, X. Zhan, Q. Peng and Z. Shuai, *J. Am. Chem. Soc.*, 2005, **127**, 6335-6346.
41. A. B. Parusel, *Phys. Chem. Chem. Phys.*, 2000, **2**, 5545-5552.
42. R. Pfattner, E. Pavlica, M. Jaggi, S. X. Liu, S. Decurtins, G. Bratina, J. Veciana, M. M. Torrent and C. Rovira, *J. Mater. Chem. C*, 2013, **1**, 3985-3988.
43. G. J. Zhao, F. Yu, M.-X. Zhang, B. H. Northrop, H. Yang, K. L. Han and P. J. Stang, *J. Phys. Chem. A*, 2011, **115**, 6390-6393.
44. Y. Zhu, R. D. Champion and S. A. Jenekhe, *Macromolecules*, 2006, **39**, 8712-8719.
45. S. Olsen and S. C. Smith, *J. Am. Chem. Soc.*, 2007, **129**, 2054-2065.
46. M. Cai, Z. Gao, X. Zhou, X. Wang, S. Chen, Y. Zhao, Y. Qian, N. Shi, B. Mi, L. Xie and W. Huang, *Phys. Chem. Chem. Phys.*, 2012, **14**, 5289-5296.
47. A. Chakraborty, S. Kar and N. Guchhait, *Chem. Phys.*, 2006, **324**, 733-741.
48. F. A. Chipem, S. Chatterjee and G. Krishnamoorthy, *J. Photoch. Photobio. A*, 2010, **214**, 121-127.
49. B. Chen, H. Nie, P. Lu, J. Zhou, A. Qin, H. Qiu, Z. Zhao and B. Z. Tang, *Chem. Commun. (Camb)*, 2014, **50**, 4500-4503.
50. T. Mutai, H. Sawatani, T. Shida, H. Shono and K. Araki, *J. Org. Chem.*, 2013, **78**, 2482-2489.
51. Y. Shigemitsu, T. Mutai, H. Houjou and K. Araki, *J. Phys. Chem. A*, 2012, **116**, 12041-12048.
52. M. Lax, *J. Chem. Phys.*, 1952, **20**, 1752-1760.
53. E. Doktorov, I. Malkin and V. Man'ko, *J. Mol. Spectrosc.*, 1977, **64**, 302-326.
54. E. Kukk, K. Ueda, U. Hergenhahn, X.-J. Liu, G. Prümper, H. Yoshida, Y. Tamenori, C. Makochekanwa, T. Tanaka and M. Kitajima, *Phys. Rev. Lett.*, 2005, **95**, 133001.
55. A. Baiardi, J. Bloino and V. Barone, *J. Chem. Theory Comput.*, 2013, **9**, 4097-4115.
56. J. Chen, A. Schmitz and D. S. Kilin, *Int. J. Quantum. Chem.*, 2012, **112**, 3879-3888.
57. A. Demeter, S. I. Druzhinin, S. A. Kovalenko, T. A. Senyushkina and K. A. Zachariasse, *J. Phys. Chem. A*, 2011, **115**, 1521-1537.
58. K. A. Zachariasse, *Chem. Phys. Lett.*, 2000, **320**, 8-13.
59. W. S. Tan, C. Prabhakar, Y.-H. Liu, S.-M. Peng and J.-S. Yang, *Photoch. Photobio. Sci.*, 2014, **13**, 211-223.
60. F. J. Avila Ferrer, J. Cerezo, J. Soto, R. Improta and F. Santoro, *Comput. Theor. Chem.*, 2014.
61. S. Ghosh, S. Horvath, A. V. Soudackov and S. Hammes-Schiffer, *J. Chem. Theory Comput.*, 2014, **10**, 2091-2102.
62. J. F. Brookes, K. M. Slenkamp, M. S. Lynch and M. Khalil, *J. Phys. Chem. A*, 2013, **117**, 6234-6243.